Atmospheric Chemistry of CF3CF2CHO: Absorption Cross Sections in the UV and IR Regions, Photolysis at 308 nm, and Gas-Phase Reaction with OH Radicals (T = 263–358 K)

4 AUTHORS, INCLUDING:

María Antiñolo
University of Castilla-La Mancha
19 PUBLICATIONS   **91** CITATIONS

SEE PROFILE

Elena Jiménez
University of Castilla-La Mancha
50 PUBLICATIONS   **497** CITATIONS

SEE PROFILE

Jose Albaladejo
Ferrer Internacional SA
76 PUBLICATIONS   **614** CITATIONS

SEE PROFILE

Atmospheric Chemistry of CF₃CF₂CHO: Absorption Cross Sections in the UV and IR Regions, Photolysis at 308 nm, and Gas-Phase Reaction with OH Radicals ($T = 263-358$ K)

María Antiñolo,[†,§] Elena Jiménez,[†,‡] Sergio González,[†] and José Albaladejo*[,†,‡]

[†]Departamento de Química Física, Facultad de Ciencias y Tecnologías Químicas, Universidad de Castilla-La Mancha, Avda. Camilo José Cela s/n, 13071 Ciudad Real, Spain

[‡]Instituto de Investigación en Combustión y Contaminación Atmosférica, Universidad de Castilla-La Mancha, Camino de Moledores s/n, Edificio Polivalente, 13071 Ciudad Real, Spain

Ⓢ Supporting Information

ABSTRACT: The relative importance in the atmosphere of UV photolysis of perfluoropropionaldehyde, CF₃CF₂CHO, and reaction with hydroxyl (OH) radicals has been investigated in this work. First, the forbidden n → π* transition of the carbonyl chromophore was characterized between 230 and 380 nm as a function of temperature (269−298 K) and UV absorption cross sections, σ_λ, were determined in those ranges. In addition, IR absorption cross sections were determined between 4000 and 500 cm⁻¹. Pulsed laser photolysis (PLP) of CF₃CF₂CHO coupled to Fourier transform infrared (FTIR) was employed to determine the overall photolysis quantum yield, Φ_λ, at 308 nm and 298 K. $\Phi_{\lambda=308\ nm}$ was pressure dependent, ranging from (0.94 ± 0.14) at 75 Torr to (0.30 ± 0.01) at 760 Torr. This dependence is characterized by the Stern−Volmer parameters $\Phi^0_{\lambda=308\ nm}$ = (1.19 ± 0.34) and K_{SV} = (1.22 ± 0.52) × 10⁻¹⁹ cm³ molecule⁻¹. End products of the photodissociation of CF₃CF₂CHO were measured and quantified by FTIR spectroscopy. Furthermore, the rate coefficients for the OH + CF₃CF₂CHO reaction, k_1, were determined as a function of temperature ($T = 263-358$ K) by PLP-LIF. At room temperature the rate coefficient is $k_1(T = 298\ K) = (5.57 \pm 0.07) \times 10^{-13}$ cm³ molecule⁻¹ s⁻¹, whereas the temperature dependence is described by $k_1(T) = (2.56 \pm 0.32) \times 10^{-12} \exp\{-(458 \pm 36)/T\}$ cm³ molecule⁻¹ s⁻¹. On the basis of our results, photolysis of CF₃CF₂CHO in the actinic region could be an important removal process for CF₃CF₂CHO in the atmosphere. The formation of the primary products in the UV photolysis of CF₃CF₂CHO is also discussed.
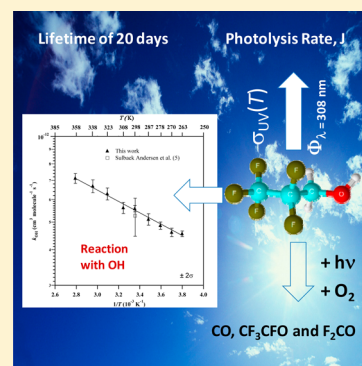
1. INTRODUCTION

Hydrochlorofluorocarbons (HCFCs) and hydrofluorocarbons (HFCs) have been used over the last decades as CFC replacements in several applications, because their ozone depletion potential (ODP) is much lower or negligible compared to CFCs. Despite the zero ODP of HFCs, in general they have high global warming potentials (GWPs) that can contribute to the greenhouse effect and potentially to climate change.[1] For that reason, other alternatives to HFCs such as hydrofluoroolefins (HFOs) or fluoroalcohols (FAs) have been considered as potential CFC replacements.[2] The atmospheric oxidation of HFOs and FAs is initiated mainly by hydroxyl (OH) radicals, producing fluorinated aldehydes as secondary pollutants. For example, Hurley et al.[3] reported that chlorine (Cl)-initiated oxidation of CF₃CF₂CH₂OH in the absence of NO yielded the perfluorinated aldehyde CF₃CF₂CHO as sole primary product. A similar mechanism is expected for the corresponding OH-reaction. The oxidation mechanism for C₄F₉CH=CH₂ and C₆F₁₃CH=CH₂ initiated by Cl atoms yielded C₄F₉CHO and C₆F₁₃CHO, respectively, as primary products.[4] By analogy with this mechanism, CF₃CF₂CHO is also expected to be formed in the atmospheric

degradation of CF₃CF₂CH=CH₂ (HFO-1345zfc). As far as we know, no product study is reported for the OH or Cl reactions with HFO-1345zfc.

The OH-reaction with perfluorinated aldehydes (PFALs) has been reported to possibly be precursors of perfluoroalkyl carboxylic acids (PFCAs, CₓF₂ₓ₊₁COOH),[5] which have been observed in biota all over the world, and are thought to be harmful.[6] Some aspects of the atmospheric chemistry of some PFALs and fluorinated aldehydes (FALs) have been reported in the literature.[5,7−15] These studies include the kinetic study of the reactivity toward OH radicals and Cl atoms,[3−5,10−13] the determination of ultraviolet (UV) and infrared (IR) absorption cross sections,[7,8,10,11,14] and the estimation of photolysis rates.[7,11,14,15] The role of UV photolysis of CF₃CF₂CHO in the atmosphere is uncertain. In the absence of quantum yield measurements, Sulbaek Andersen et al.[5] reported that CF₃CF₂CHO was likely to be removed by photolysis in a few weeks, while Chiappero et al.[7] estimated that the lifetime of

CF$_3$CF$_2$CHO with respect to photolysis was less than 2 days at 40° latitude, assuming a constant photolysis quantum yield of 0.11 (i.e., independent of pressure and wavelength).

The aim of this work is to evaluate the significance of OH reaction over the photolysis loss of CF$_3$CF$_2$CHO in the atmosphere. UV and IR absorption cross sections, σ_λ(230–380 nm) and $\sigma(\tilde{v} = 500$–4000 cm^{-1}), were determined for CF$_3$CF$_2$CHO by gas-phase UV and Fourier transform infrared (FTIR) absorption spectroscopy, respectively. Additionally, the overall photolysis quantum yield of CF$_3$CF$_2$CHO at 308 nm, $\Phi_{\lambda=308\text{ nm}}$, was determined for the first time as a function of pressure (P = 75–760 Torr of air) by pulsed laser photolysis coupled to FTIR spectroscopy (PLP–FTIR). Photooxidation end-products were also detected in situ during the PLP of CF$_3$CF$_2$CHO samples.

Furthermore, the absolute rate coefficient for the OH-reaction with CF$_3$CF$_2$CHO (k_1) as a function of temperature (T = 263–358 K) was determined here for the first time by monitoring OH radicals by the laser-induced fluorescence (LIF) technique.

$$\text{OH} + \text{CF}_3\text{CF}_2\text{CHO} \rightarrow \text{H}_2\text{O} + \text{CF}_3\text{CF}_2\text{CO} \tag{1}$$
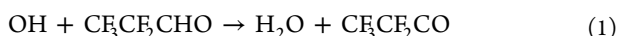
The reported parameters (σ_λ, Φ_λ, and k_1) allow the estimation of the relative importance of photolysis of CF$_3$CF$_2$CHO in the actinic region over its removal by reaction with OH radicals in the atmosphere. The molar yields of some primary products and a possible explanation for the formation of secondary products are also reported.

2. EXPERIMENTAL SECTION

Because different setups have been used in this kinetic and photochemical study, this section is divided into four subsections.

2.1. Synthesis of Gaseous CF$_3$CF$_2$CHO. CF$_3$CF$_2$CHO is easily hydrated and for that reason is commercially available in the stable hydrated form, CF$_3$CF$_2$CH(OH)$_2$, which is a crystalline solid (Apollo Scientific Ltd., >90%, mp = 52–53 °C).[16] The dehydration procedure was similar to that described by Braid et al.[17] A 10 g amount of molten CF$_3$CF$_2$CH(OH)$_2$ was dropped slowly into a flask containing 25 g of phosphorus pentoxide, P$_2$O$_5$ (Fluka, >99.9%). The content of the flask was heated at 60 °C and vigorously stirred. A continuous flow of He of 20 standard cubic centimeter per minute (sccm) was introduced through the flask to carry gaseous CF$_3$CF$_2$CHO (bp = 2 °C at 746 Torr)[16] to a trap cooled with liquid nitrogen. A stainless steel gas bottle was used to store the aldehyde at room temperature. IR analysis of the crude sample of CF$_3$CF$_2$CHO collected in the trap did not reveal the presence of a significant amount of impurities.

2.2. UV and FTIR Absorption Spectroscopy. The UV absorption spectra were measured between 230 and 380 nm at different temperatures (269–298 K) using an apparatus described previously.[18,19] It consists of a deuterium lamp as irradiation source, a Pyrex absorption cell (l = 107 cm), and a 0.5-m spectrograph equipped with a coupled-charge device (CCD) as a detector. The instrumental resolution of the spectrograph was 0.17 nm. The wavelengths were daily calibrated prior use with a pen-ray Hg lamp. The temperature inside the cell was regulated by ethanol circulating through an outer jacket by using a thermostatic bath (Huber, Polystat CC1). The measurements were performed under static conditions, filling the cell with pure CF$_3$CF$_2$CHO (0.5–9.8 Torr). The range of concentrations inside the absorption cell

was calculated from the measured pressures and temperature (1.62 × 10^{16} to 3.18 × 10^{17} molecules cm^{-3}). A reference spectrum was recorded before each measurement. The determination of the UV absorption cross sections (base e), σ_λ, was based on the Beer–Lambert Law ($A(\tilde{v}) = \sigma(\tilde{v}) l[\text{CF}_3\text{CF}_2\text{CHO}]$). σ_λ was obtained from the slope of the absorbance at a given wavelength λ versus CF$_3$CF$_2$CHO pressure. Some examples of these plots are depicted in Figure S1 of the Supporting Information.

IR absorption cross sections, $\sigma(\tilde{v})$, were determined between 500 and 4000 cm^{-1} with an experimental setup previously described.[13,20,21] A multipass gas cell with a path length of 8 m coupled to a FTIR spectrometer (Bruker, Tensor 27) with N$_2$-liquid cooled mercury cadmium telluride (MCT) detector was used to measure the IR absorption spectrum of the sample. The resolution of the recorded spectra was 1 cm^{-1}. The measurements were carried out exclusively at room temperature and under static conditions from diluted mixtures of CF$_3$CF$_2$CHO in helium. Dilution factors, f, are defined as the ratio of CF$_3$CF$_2$CHO partial pressure, $p(\text{CF}_3\text{CF}_2\text{CHO})$, and the total pressure in the bulb, $p_T = p(\text{CF}_3\text{CF}_2\text{CHO}) + p_{\text{He}}$. f values ranged from 0.01% to 0.09%. Total pressures inside the absorption cell were varied from 5 to 50 Torr. Initial concentrations of CF$_3$CF$_2$CHO were determined from the partial pressure $p(\text{CF}_3\text{CF}_2\text{CHO})$ inside the cell ([CF$_3$CF$_2$CHO] = (0.3–7.6) × 10^{14} molecules cm^{-3}). Optical saturation was not reached at the concentration level used, and the Beer–Lambert Law was accomplished in the whole range, i.e., a linear relationship between the absorbance and the concentration was observed.

2.3. PLP–FTIR System: $\Phi_{\lambda=308\text{ nm}}$ Determination. The PLP–FTIR system was described in previous works.[14,15] A cylindrical photolysis cell (L = 10 cm, d = 2 cm) was filled under static conditions with a diluted mixture of CF$_3$CF$_2$CHO (f = 0.13–0.25%) in air (p_T = 75–760 Torr). An excess of cyclohexane ([C$_6$H$_{12}$]$_0$/[CF$_3$CF$_2$CHO]$_0$ = 25–46) was added to the gas mixture to scavenge OH radicals possibly formed in the system (see section 3). The sample was photolyzed at 308 nm by a pulsed XeCl excimer laser, operating at a repetition rate that ranged between 1 and 10 Hz. The number of pulses, n, was varied between 300 and 2400. A cylindrical lens (−40 mm focal length) was placed between the laser and the cell to expand the laser beam and completely irradiate the gas cell. Spectra of the fresh and photolyzed sample were recorded through the FTIR spectroscopy setup described in subsection 2.2 and after the expansion of the content of the photolysis cell into the IR gas cell. The loss of CF$_3$CF$_2$CHO by photo-dissociation can be described by a first-order rate law. The carbonyl band of the perfluorinated aldehyde was used to monitor its temporal decay. As described previously,[15] for fractional photolysis below 10^{-4} molecule pulse^{-1}, the integrated rate equation can be expressed in terms of integrated absorbances of CF$_3$CF$_2$CHO (A_n) as:

$$\ln\left(\frac{A_0}{A_n}\right) = J_\lambda \frac{n}{v_{\text{rep}}} \tag{2}$$

where A_0 and A_n are the integrated absorbances of the fresh (n = 0) and photolyzed samples, respectively, and v_{rep} is the repetition rate of the photolysis laser. The photolysis rate, J_λ, was determined as a function of total pressure from the slope of the plot of $\ln(A_0/A_n)$ versus n. This parameter is defined as:

$$J_\lambda = \Phi_\lambda \sigma_\lambda F_\lambda \qquad (3)$$

The laser fluence, F_λ, at 308 nm was obtained by chemical actinometry using acetaldehyde (CH_3CHO). At a constant F_λ (varied from 1.0×10^{16} to 2.1×10^{17} photon cm^{-2} s^{-1}), the photolysis quantum yield of CF_3CF_2CHO at 308 nm can then be obtained from the following equation:

$$\Phi_{CF_3CF_2CHO} = \Phi_{CH_3CHO} \frac{J_\lambda(CF_3CF_2CHO) \times \sigma_{CH_3CHO}}{J_\lambda(CH_3CHO) \times \sigma_{CF_3CF_2CHO}} \qquad (4)$$

The photodissociation quantum yield and the absorption cross section at 308 nm for CH_3CHO were taken from the literature as 0.29 at 1 bar and 3.33×10^{-20} cm^2 $molecule^{-1}$, respectively.[22,23]

2.4. PLP–LIF System: Gas-Phase OH Kinetics. As previously described,[24−26] a Pyrex-jacketed reaction cell ($V = 200$ cm^3) was used. Diluted CF_3CF_2CHO, OH-precursor (HNO_3), and helium were flowed through the cell by means of calibrated mass flow controllers. Total flow rate ranged between 210 and 550 sccm. Pressure inside the cell ($p_T = 50−205$ Torr) was controlled by a needle valve and measured by a capacitance manometer from Leybold Vacuum (CERAVAC CTR90 for pressures up to 100 Torr and SKY CM 1000 for pressures up to 1000 Torr). Flow rates and total pressure measurements were used to determine the concentration of CF_3CF_2CHO inside the cell ([CF_3CF_2CHO] = $(0.2−7.4) \times 10^{15}$ molecules cm^{-3}). A cooling (ethanol) or heating liquid (water) was flowed through the reactor jacket to vary the temperature inside the cell between 263 K and 358 K. OH radicals were generated by the pulsed photolysis of gaseous HNO_3 at 248 nm using a KrF excimer laser at a repetition rate of 10 Hz. Gaseous HNO_3 was obtained by bubbling helium through an aqueous solution of HNO_3 (1−5 sccm).

Gas-phase concentration of HNO_3 ($(0.5−1.8) \times 10^{15}$ molecules cm^{-3}) and initial OH concentrations, $[OH]_0$, ($(1.0−4.2) \times 10^{11}$ radical cm^{-3}) inside the cell were estimated as described in previous works.[18,20] The initial OH radical concentration, $[OH]_0$, was estimated from the relationship:

$$[OH]_0 = F_{248nm} \phi_{OH} \sigma_{248nm} [HNO_3]_0 \qquad (5)$$

where $\sigma_{248 nm}$ is the absorption cross section at 248 nm of HNO_3 (2.03×10^{-20} cm^2 $molecule^{-1}$),[27] ϕ_{OH} is the OH quantum yield of the precursor ($\phi_{OH} = 0.97$),[27] and $F_{248 nm}$ is the photolysis laser fluence at the photolysis wavelength.

The decay of OH radicals was monitored by LIF. A doubled-frequency dye laser pumped by a Nd:YAG laser was used to excite OH radicals at 282 nm. LIF signal was detected by a filtered photomultiplier tube placed orthogonally to both laser sources (Oriel, band-pass filter with 90% of transmission at 350 nm and fwhm of 150 nm). The LIF signal was transferred to a computer and analyzed as described previously.[24] The pseudo-first-order conditions were accomplished ([$CF_3CF_2CHO]_0$/$[OH]_0 = 800−52000$ and $[HNO_3]_0/[OH]_0 = 3670−6270$). The pseudo-first-order rate coefficient (k') was obtained at each reactant concentration. k' is defined as follows:

$$k' = k_1[CF_3CF_2CHO] + k_0 \qquad (6)$$

where k_0 is the first-order OH loss in absence of CF_3CF_2CHO including the OH loss due to diffusion out of the detection zone and the reaction with HNO_3.

Reagents. Cyclohexane (Aldrich, 99.9%) and CH_3CHO (Sigma-Aldrich, ≥99.5%) were degassed by freeze−pump−

thaw cycles prior to use. HNO_3 (Panreac, 65%) was used as supplied. Gases from Praxair were used also as supplied: synthetic air (99.999%) and He (99.999%).

3. RESULTS AND DISCUSSION

This section has been divided into three subsections for ease of presentation. The first subsection presents the results and discussion of the UV and IR absorption cross sections of CF_3CF_2CHO. In subsection 3.2, the photodissociation quantum yield of this fluorinated aldehyde is reported as a function of total pressure together with the detected photo-oxidation products. Lastly, the observed temperature dependence of the rate coefficients for reaction 1 is reported. A comparison with CH_3CH_2CHO and partially fluorinated propanals is also included in the discussion on both the photolysis and the reactive processes.

Unless otherwise stated, uncertainties are at 95% confidence level ($\pm 2\sigma$) where the standard deviation represents only the precision of the measurement. Systematic errors have been estimated to be $\pm 6\%$.

3.1. UV and IR Absorption Cross Sections. Averaged UV absorption cross sections at temperatures between 269 K and 298 K for CF_3CF_2CHO are presented in Table S1 of the Supporting Information and depicted in Figure 1a as well. A weak absorption band was observed corresponding to the forbidden $n \rightarrow \pi^*$ transition of the carbonyl chromophore. An averaged 5% increase of σ_λ with temperature was observed between 230 and 380 nm. Chiappero et al.[7] also reported a negligible variation (<5%) of σ_λ as a function of temperature between 249 K and 297 K, as we observed.

At all temperatures, the maximum absorption cross section is located around 308 nm. The average of the maximum absorption wavelength is (308.13 ± 0.76) nm. In Table 1 a summary of the maximum absorption λ and $\sigma_{\lambda,max}$ is presented for comparison with literature data. As can be seen, there is a good agreement, considering the uncertainties, with σ_λ reported by Chiappero et al.[7] and Hashikawa et al.[8] The discrete absorption cross sections from Borkowski and Ausloos[28] and Pitchard et al.[29] were not determined at the maximum absorption peak, as can be seen in Figure 1b.

The averaged IR absorption cross sections, $\sigma(\tilde{v})$ (base e), are presented in Table S2 of the Supporting Information and depicted in Figure 2 together with those reported by Hashikawa et al.[8] In Figure 2a, the 1500−1000 cm^{-1} region corresponding to complex normal modes that include H−C−O bending or C−F stretching is shown. As can be seen in Figure 2, $\sigma(\tilde{v})$ reported by Hashikawa et al.[8] are in good agreement with those determined in this work. Only for the absorption peak in the 1500−1000 cm^{-1} region, which is located at 1224.2 cm^{-1}, Hashikawa et al.[8] reported $\sigma(\tilde{v})_{max}$ approximately 5% higher than ours. The band centered at 1775.8 cm^{-1} is characteristic of the carbonyl group in aldehydes. The observed difference in $\sigma(\tilde{v})_{max}$ is within the uncertainty of the measurements.

The main contribution to the systematic errors in the reported parameters σ is the uncertainty in the CF_3CF_2CHO concentration that was estimated to be less than $\pm 5\%$.

3.2. Pulsed Photolysis of CF_3CF_2CHO at 308 nm in the Presence of Air. *3.2.1. Quantum Yields as a Function of Total Pressure.* After absorption of 308 nm radiation, excited CF_3CF_2CHO (denoted by an asterisk) can undergo photodissociation via the following three thermodynamically possible channels:
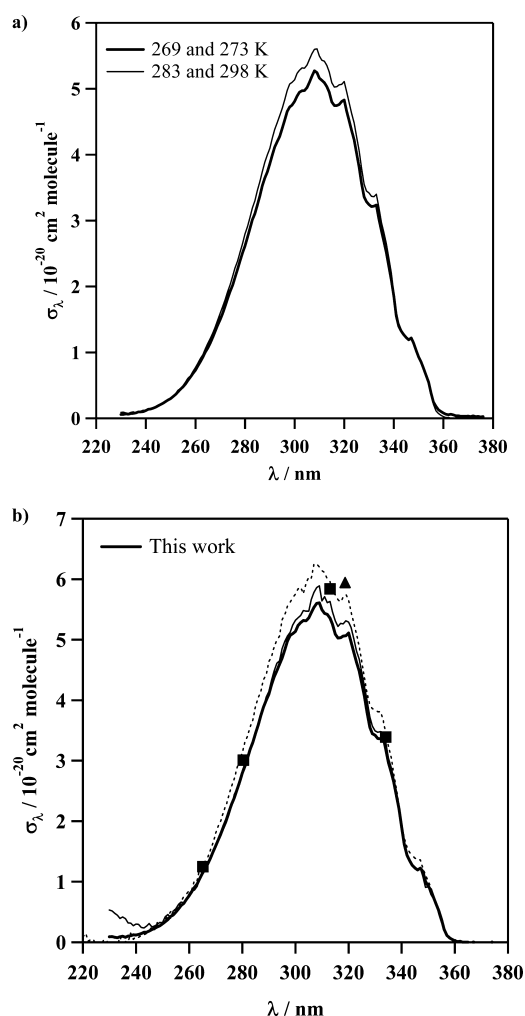
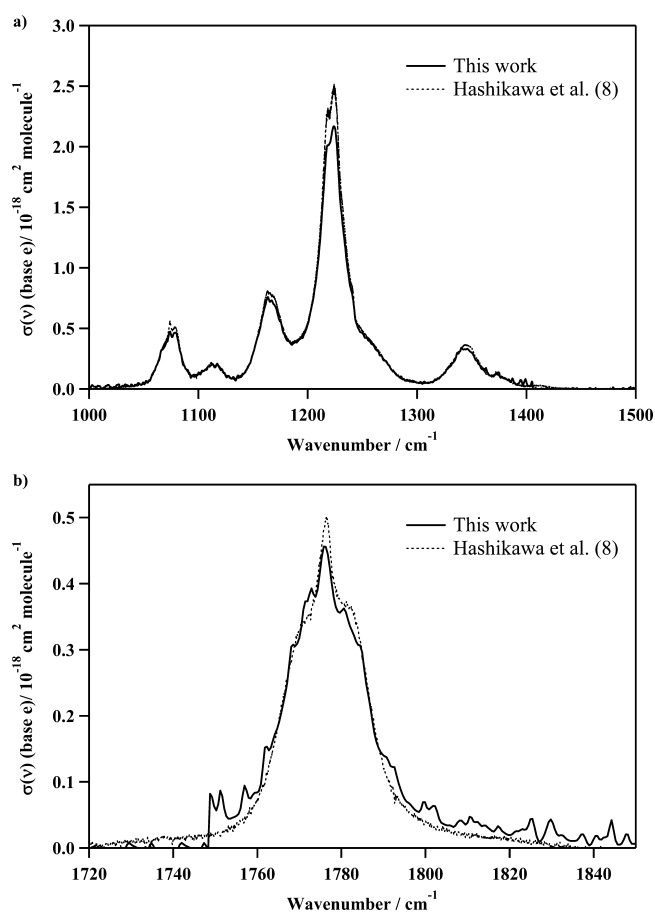Figure 1. (a) Average UV absorption cross sections of CF_3CF_2CHO at temperatures between 269 K and 298 K. (b) Comparison of the UV absorption spectrum obtained in this work at room temperature with previous studies (■ from Borkowski and Ausloos;[28] ▲ from Pritchard et al.;[29] dashed line from Chiappero et al.;[7] dotted line from Hashikawa et al.[8]).

Table 1. Peak UV Absorption Cross Sections and Maximum Absorption Wavelength for CF_3CF_2CHO

| T, K	λ_{max}, nm	σ_λ, 10^{-20} cm^2 molecule^{-1}	reference
269−273	308.3 ± 0.4	5.29 ± 0.30	this work
283−298	308.4 ± 0.6	5.60 ± 0.22	this work
298	309	5.89	Chiappero et al.[7]
298	307−308	6.25	Hashikawa et al.[8]

$$CF_3CF_2CHO^* \rightarrow HCO + CF_3CF_2 \qquad (7a)$$

$$\rightarrow CO + CF_3CF_2H \qquad (7b)$$

$$\rightarrow H + CF_3CF_2CO \qquad (7c)$$

Figure 3a shows an example of the recorded IR spectrum before irradiation of a CF_3CF_2CHO/cyclohexane/air mixture. After irradiation of the sample with 1200 laser pulses and subtraction of CF_3CF_2CHO and cyclohexane features, the residual IR spectrum obtained is depicted in Figure 3b. The identified products were CO, CF_3CFO, F_2CO and small amounts of HCOOH. The carbonyl band from HCOOH

Figure 2. IR absorption cross sections of CF_3CF_2CHO (in base e) recorded (a) between 1500 and 1000 cm^{-1} and (b) for the carbonyl band at 1 cm^{-1} resolution and 298 K. The results reported by Hashikawa et al.[8] are also depicted for comparison purposes.
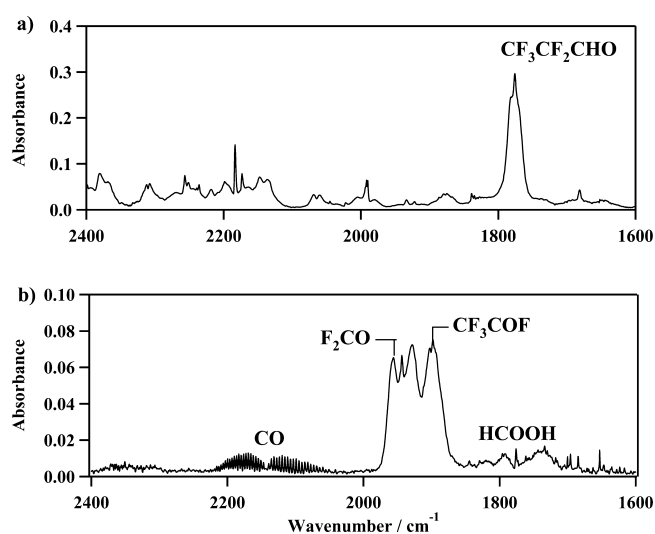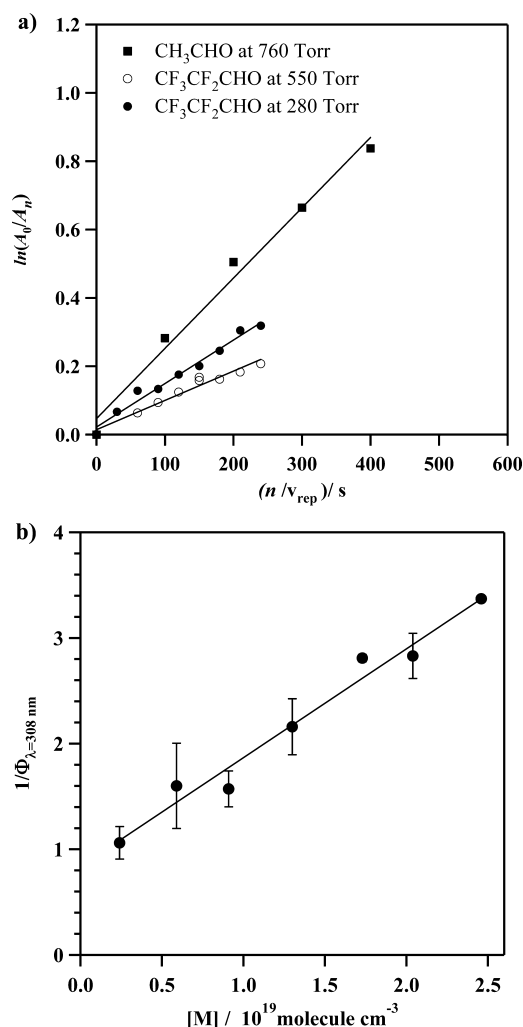

Figure 3. FTIR spectra of CF_3CF_2CHO (2.6×10^{16} molecules cm^{-3} in the photolysis cell) in the presence of cyclohexane (1.2×10^{18} molecules cm^{-3} in the photolysis cell) at 630 Torr of air (a) before irradiation, and (b) after 1200 laser pulses at 1.4×10^{17} photon cm^{-2} s^{-1} (CF_3CF_2CHO and cyclohexane features were subtracted from the spectrum).

overlaps with that of CF_3CF_2CHO, interfering in the measurements of A_n. For that reason, at high initial

CF_3CF_2CHO concentrations, A_0 and A_n were measured using the 759–674 cm^{-1} band (band strength of 2.17×10^{-18} cm^2 $molecule^{-1}$ cm^{-1}), where no interference of HCOOH existed. In contrast, at low initial CF_3CF_2CHO concentrations, the analysis of A_0 and A_n was performed by using the intense carbonyl band (band strength of 3.85×10^{-18} cm^2 $molecule^{-1}$ cm^{-1} between 1837 and 1716 cm^{-1}).

A plot of $\ln(A_0/A_n)$ versus n for CH_3CHO at 760 Torr and for CF_3CF_2CHO at 280 and 550 Torr are shown in Figure 4a

Table 2. Photolysis Quantum Yields for CF_3CF_2CHO in Air at 308 nm

P_T, Torr	$[M] \times 10^{-19}$/molecules cm^{-3}	$\Phi_{\lambda=308\ nm}$
75	0.24	0.94 ± 0.14
181	0.59	0.63 ± 0.16
281	0.91	0.64 ± 0.07
402	1.30	0.46 ± 0.06
535	1.73	0.36 ± 0.01
631	2.04	0.35 ± 0.03
760	2.46	0.30 ± 0.01

where K_{SV} is the Stern–Volmer constant and $\Phi^0_{\lambda=308\ nm}$ is the quantum yield in the absence of a quencher, i.e., at zero pressure. In Figure 4b the Stern–Volmer plot is shown for $\Phi_{\lambda=308\ nm}$. The parameters obtained from the linear least-squares regression of the data were $\Phi^0_{\lambda=308\ nm} = (1.19 \pm 0.34)$ and $K_{SV} = (1.22 \pm 0.52) \times 10^{-19}$ cm^3 $molecule^{-1}$. The Stern–Volmer parameters were used to derive the photodissociation quantum yield of CF_3CF_2CHO at tropospheric pressures (see section 4). Systematic errors in Φ_λ are associated to the accuracy of the photodissociation quantum yield of CH_3CHO ($\pm5\%$), the precision of the UV absorption cross sections of CF_3CF_2CHO at 308 nm ($\pm1\%$), and the uncertainty in the measurement of the IR integrated areas ($\pm5\%$). These systematic uncertainties contribute less than $\pm5\%$ to the total uncertainty.

At 760 Torr and 298 K, the photolysis quantum yield of CF_3CF_2CHO at 308 nm can be compared with that of CH_3CH_2CHO, CF_3CH_2CHO, and CF_3CHO. The IUPAC recommendation for the photolysis quantum yield for CH_3CH_2CHO in air at 1 bar and 298 K is around unity and independent of wavelength between 280 and 310 nm.[26] In our previous work on the photolysis of CF_3CH_2CHO at 308 nm, it was concluded that the substitution of a CH_3 group by a CF_3 provokes a dramatic reduction on the quantum yield (from 1 to 0.023).[14] This decrease in $\Phi_{\lambda=308\ nm}$ is less pronounced for CF_3CHO (0.17)[7] with respect to CH_3CHO (0.29).[25] It is worth noting that if the CH_2 group in CF_3CH_2CHO is substituted by a CF_2 group, an increase in the photodissociation quantum yield is observed (from 0.023 to 0.30 at 760 Torr of air).

3.2.2. Photolysis Products in the Presence of Air. In contrast to what Chiappero et al.[7] observed at 254 nm, CF_3CF_2H was not detected in the IR spectra recorded after photolysis of CF_3CF_2CHO at 308 nm. These authors reported that CF_3CF_2 radicals (channel in eq 7a) and CF_3CF_2H (channel in eq 7b) were equally important (ca. 50% of Φ_λ). In our study, the photolysis channel eq 7b seems to be negligible. Therefore, CO is expected to be mainly formed from the reaction of HCO radicals, from the channel eq 7a, with O_2:

$$HCO + O_2 \rightarrow CO + HO_2 \qquad (9)$$
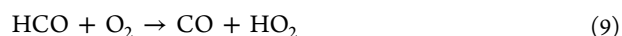
CO has been detected in this work but it was not quantified, because it can be formed by unavoidable secondary chemistry. Therefore, in the present study, only CF_3CFO and F_2CO were quantified by spectral subtraction of reference spectra of known concentration. Reference spectra of F_2CO and CF_3CFO were provided by I. Barnes[30] and T. J. Wallington,[31] respectively. Given the small amounts of HCOOH detected, the quantification of this species was subject to large uncertainties, and results were in most cases too scattered to provide a reliable yield for this minor product. To be conservative, an

Figure 4. (a) Temporal decays of CF_3CF_2CHO (at 280 and 550 Torr of air) and the actinometer CH_3CHO (at 760 Torr of air) in the photolysis process at 308 nm. (b) Stern–Volmer plot between 75 and 760 Torr for the photolysis quantum yield of CF_3CF_2CHO at 308 nm.

$(F_\lambda = 5.2 \times 10^{16}$ photon cm^{-2} $s^{-1})$. An increase of the slope of these plots for CF_3CF_2CHO, i.e., $\Phi_{\lambda=308\ nm}$ according to eq 2 and eq 3, was observed at lower pressures. The averaged values of $\Phi_{\lambda=308\ nm}$ at pressures between 75 and 760 Torr and room temperature are summarized in Table 2. The observed effect of total pressure on $\Phi_{\lambda=308\ nm}$ can be explained by a Stern–Volmer mechanism. Collisional deactivation of $CF_3CF_2CHO^*$ by air is competing with the photodissociation process. If no other photophysical process is competing, a Stern–Volmer behavior is expected for the photolysis quantum yield $\Phi_{\lambda=308\ nm}$:

$$\frac{1}{\Phi_{\lambda=308\ nm}} = \frac{1}{\Phi^0_{\lambda=308\ nm}} + \frac{K_{SV}}{\Phi^0_{\lambda=308\ nm}}[M] \qquad (8)$$
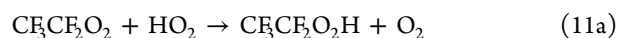
upper limit of 0.07 can be reported for the molar yield of HCOOH. Figure 5 shows the evolution of CF_3CFO and F_2CO
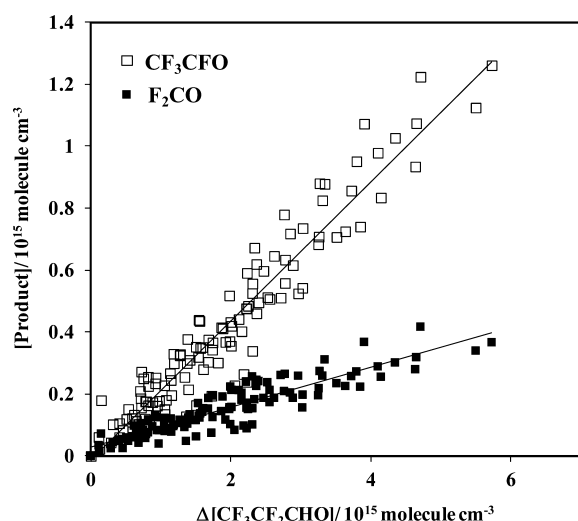

Figure 5. Plots of CF_3CFO and F_2CO formation as a function of CF_3CF_2CHO loss for all total pressures studied.

formation observed for all experiments carried out, i.e., plots of $[CF_3CFO]$ and $[F_2CO]$ versus CF_3CF_2CHO loss $(\Delta[CF_3CF_2CHO])$. The molar yield of CF_3CFO and F_2CO was measured to be (0.21 ± 0.08) and (0.07 ± 0.04), respectively.

Formation of CF_3CFO can be due to reaction of CF_3CF_2 radicals from the channel shown in eq 7a with O_2 and further reaction with HO_2 radicals:[27]

$$CF_3CF_2 + O_2 + M \rightarrow CF_3CF_2O_2 + M \tag{10}$$

$$CF_3CF_2O_2 + HO_2 \rightarrow CF_3CF_2O_2H + O_2 \tag{11a}$$

$$\rightarrow CF_3CFO + HOF + O_2 \tag{11b}$$

Halogenated peroxy radicals formed in reaction 10 can also undergo self-reaction:

$$2CF_3CF_2O_2 \rightarrow 2CF_3CF_2O + O_2 \tag{12}$$
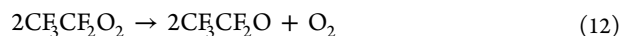
Subsequent disproportionation of CF_3CF_2O can produce F_2CO:

$$CF_3CF_2O + M \rightarrow CF_3 + F_2CO + M \tag{13}$$

The observed molar yield of F_2CO is much lower than that of CF_3CFO, which is consistent with the predominance of reaction 11 over reaction 12.

If CF_3CF_2CO radicals were formed in the channel shown in eq 7c, CF_3CF_2COOH could be formed in a similar way, as $CF_3(CH_2)_xCOOH$ is formed in the presence of O_2 and HO_2:[14,15]

$$CF_3CF_2CO + O_2 + M \rightarrow CF_3CF_2C(O)O_2 + M \tag{14}$$

$$CF_3CF_2C(O)O_2 + HO_2 \rightarrow CF_3CF_2COOH + O_3 \tag{15}$$
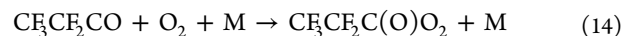
No detectable amounts of CF_3CF_2COOH were found in this work, maybe because of thermal decomposition of CF_3CF_2CO and $CF_3CF_2C(O)O_2$ radicals:

$$CF_3CF_2CO + M \rightarrow CF_3CF_2 + CO + M \tag{16}$$

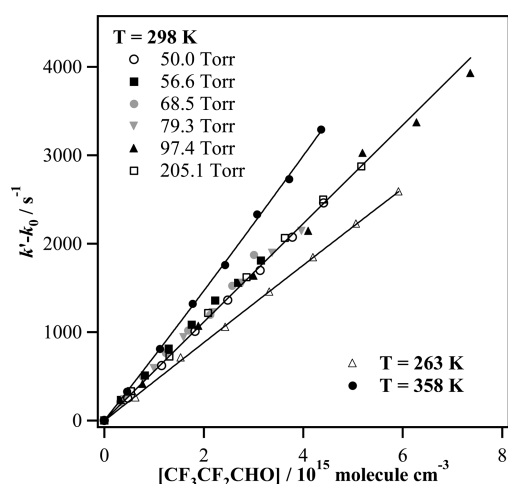$$CF_3CF_2C(O)O_2 + M \rightarrow CF_3CF_2O + CO_2 + M \tag{17}$$
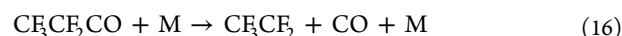
Hurley et al.[32] estimated that disproportionation reaction of CF_3CF_2CO accounts for 52% of its loss under atmospheric conditions. Moreover, Setokuchi et al.[33] calculated at 760 Torr and 298 K that the thermal decomposition rate for CF_3CF_2CO was around 10^6 s^{-1} and the yield of CO could range from 23% to 36%. An upper limit contribution of 4% can be reported for the CF_3CF_2COOH formation via the channel eq 7c, by comparing with a reference IR spectrum. In conclusion, the main photolysis channel for CF_3CF_2CHO at 308 nm is shown in eq 7a, forming HCO and CF_3CF_2 radicals. The channels shown in eqs 7b and 7c seem to be negligible at this wavelength.

3.3. OH-Reaction Rate Coefficients. Examples of temporal decays of the LIF signal in the absence and presence of CF_3CF_2CHO are presented in Figure S2 of the Supporting Information. From the analysis of the LIF decays at $[CF_3CF_2CHO] = 0$, k_0 (99−260 s^{-1}), which includes the reaction of OH with HNO_3 and diffusion out of the detection zone, was obtained at each temperature. Similarly, k' values ranging from 265 to 4027 s^{-1} were obtained in the presence of different CF_3CF_2CHO concentrations. The experimental conditions employed and the averaged rate coefficients obtained at all temperatures are tabulated in Table 3.

The contribution of k_0 in k' varies between 3% and 55%, although typically was around 20%. k_1 at each temperature was obtained from the slope of $k' - k_0$ versus $[CF_3CF_2CHO]$ plots according to eq 6. In Figure 6 examples of those plots are shown for 298 K as a function of total pressure (50−205 Torr) together with an example at 263 and 358 K. No dependency of

Table 3. Experimental Conditions Employed in the Kinetic Study of the Reaction of OH with CF_3CF_2CHO Together with the Pseudo-First-Order Ranges and the Absolute Rate Coefficient Obtained at Each Temperature

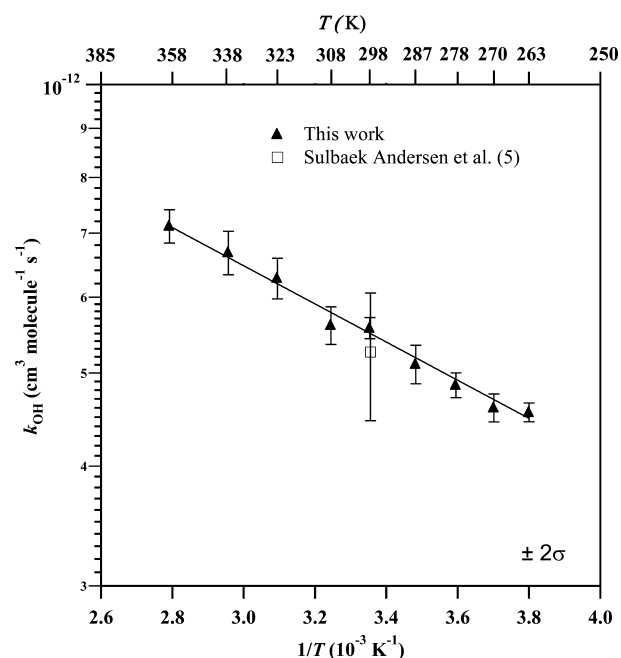| T, K	p_T, Torr	F_T, sccm	$[CF_3CF_2CHO]$, 10^{15} molecules cm^{-3}	$[HNO_3]$, 10^{15} molecules cm^{-3}	$F_{248\ nm}$, mJ pulse^{-1} cm^{-2}	$[OH]_0$, 10^{11} radical cm^{-3}	k_0, s^{-1}	k_1', s^{-1}	$k_1(T) \times 10^{13}$, cm^3 molecule^{-1} s^{-1}
263	51.7−81.2	212−338	0.4−6.6	0.5−0.9	6.7−9.9	1.3−1.7	230−121	333−4027	4.55 ± 0.09
270	49.8−75.0	213−338	0.3−5.9	0.5−1.0	8.2−9.8	1.1−1.9	184−99	305−2746	4.60 ± 0.08
278	51.9−90.1	212−285	0.4−6.9	0.8−1.4	7.2−10.8	1.9−2.6	97−183	265−2800	4.86 ± 0.07
287	60.2−91.8	212−336	0.4−5.5	0.7−1.1	8.4−10.7	1.4−2.8	260 −134	309−3433	5.11 ± 0.12
298	50.3−205.1	211−548	0.3−7.4	0.8−1.6	5.8−10.6	1.3−4.2	173−113	369−2817	5.57 ± 0.07
308	64.0−91.6	212−336	0.4−6.5	1.0−1.5	8.5−11.1	1.0−1.5	194 −140	371−3625	5.61 ± 0.13
323	51.7−84.7	211−314	0.2−4.4	1.1−1.4	7.5−9.9	1.1−1.4	162 −135	308−2708	6.28 ± 0.15
338	61.8−86.9	211−335	0.3−4.6	1.3−1.5	6.5−9.3	1.3−1.5	163−141	359−2977	6.68 ± 0.17
358	63.0−95.5	211−335	0.3−5.4	1.7−1.8	7.3−9.2	1.7−1.8	178−168	404−3805	7.12 ± 0.14

Figure 6. $k' - k_0$ plots versus $[CF_3CF_2CHO]$ at different pressures between 50 and 205 Torr at 298 K. An example of these plots at 263 K and 358 K are also displayed.

Figure 7. Arrhenius plot for the OH-rate coefficient of the reaction with CF_3CF_2CHO between 263 K and 358 K. Error bars represent uncertainties at $\pm 1\sigma$ level.

k_1 on total pressure is observed at the studied range. Therefore, the linear least-squares fit of all the room temperature data allowed to obtain $k_1(298\ K) = (5.57 \pm 0.07) \times 10^{-13}$ cm^3 molecule^{-1} s^{-1}. This value is in a very good agreement with the only one previous study,[5] as can be seen in Table 4. The Arrhenius plot of these data is depicted in Figure 7. The Arrhenius equation derived from the exponential fit of the data from Table 3 is the following:

$$k_1(T) = (2.56 \pm 0.32) \times 10^{-12} \exp\{-(458 \pm 36)/T\}$$
$$\text{cm}^3 \text{ molecule}^{-1} \text{ s}^{-1} \quad (18)$$

Systematic uncertainties in $k_{OH}(T)$ can be associated mainly to the purity of the sample, which could enhance the secondary chemistry, and other experimental parameters such as temperature and pressure. Even though, no detectable amounts of potential sample impurities were observed in the infrared measurements an uncertainty of $\pm 5\%$ has been considered, taking into account the difference in $\sigma(\tilde{\nu})$ and σ_λ determined in this work with previous studies. Uncertainties in the pressure and temperature measurements contribute less than $\pm 1\%$ to the overall uncertainty in CF_3CF_2CHO concentration. On the basis of these considerations and being conservative, we estimate an overall uncertainty in $k_{OH}(T)$ of $\pm 10\%$, and therefore it must be added to the uncertainties stated in Tables 2 and 3.

Kinetic parameters for the OH-reaction with CF_3CF_2CHO are summarized in Table 4, together with those for other aldehydes from the literature. At room temperature, the OH-reactivity of CF_3CHO, CF_3CF_2CHO, and $CF_3(CF_2)_2CHO$ is

very similar, because these species contain only one hydrogen atom from the CHO group susceptible to be abstracted by OH radicals. As can be seen in Table 4, abstraction of H atom from CHO group is highly deactivated by the presence of F atoms, and a decrease in $k_{OH}(298\ K)$ was observed as in the series CH_3CH_2CHO,[26] CF_3CH_2CHO,[13] and CF_3CF_2CHO. The activation energies (expressed as E_a/R) for C$_3$ and C$_4$ aldehydes are similar, within the uncertainties given, and pre-exponential factor (A) are on the order of 10^{-12} cm^3 molecule^{-1} s^{-1}. A and E_a for the OH+CF_3CHO reaction have not been reported, as far as we know, but they are expected to be on the same order of magnitude as that for CF_3CF_2CHO, because adding CF$_2$ groups to the molecule has a negligible effect on k_{OH}. The similar positive temperature dependence observed for these C$_3$ and C$_4$ aldehydes can be indicative of a similar reaction mechanism, presumably a H-abstraction for the CHO group.[34]

4. ATMOSPHERIC IMPLICATIONS

In this work, the tropospheric lifetimes due to photolysis ($\tau_{h\nu}$) and OH radical reaction (τ_{OH}) were estimated to evaluate the relative importance of both removal pathways for CF_3CF_2CHO in the atmosphere. τ_{OH} was estimated as in previous works by using the expression given by eq 19:[20]

Table 4. Comparison of the OH Rate Coefficient for CF_3CF_2CHO with Other Perfluorinated and Hydrogenated Aldehydes from the Literature

aldehyde	T, K	$k_{OH}(298\ K) \times 10^{13}$, cm^3 molecule^{-1} s^{-1}	$A \times 10^{12}$, cm^3 molecule^{-1} s^{-1}	(E_a/R), K	technique[a]	reference
CF_3CHO	298	5.70 ± 0.02	n.m.	n.m.		Atkinson et al.[37]
CF_3CF_2CHO	263−358	5.57 ± 0.07	2.56 ± 0.32	458 ± 36	PLP−LIF	this work
	298	5.26 ± 0.80	n.m.	n.m.	RR−FTIR	Sulbaek Andersen et al.[5]
CF_3CH_2CHO	263−358	25.9 ± 5.0	7.8 ± 2.2	314 ± 90	PLP−LIF	Antiñolo et al.[13]
CH_3CH_2CHO	240−380	200	5.1	405		Atkinson et al.[26]
$CF_3(CF_2)_2CHO$	252−273	5.80 ± 0.60	2.0 ± 0.6	369 ± 90	PLP−LIF	Solignac et al.[10]

[a]PLP-LIF, pulsed-laser photolysis with laser-induced fluorescence; RR-FTIR, relative rate with FTIR detection; n.m., not measured.

184

dx.doi.org/10.1021/jp410283v | J. Phys. Chem. A 2014, 118, 178−186

$$\tau_{OH} = \frac{1}{k_{OH}(T = 275 \text{ K})[OH]_{avg}} \tag{19}$$

$[OH]_{avg}$ is the global average concentration of OH radicals in the troposphere and was taken as 1×10^6 molecules cm^{-3}.[35] A temperature of 275 K is preferred in the lifetime estimation in order to use a tropospheric averaged lifetime. This implies the use of $k_{OH}(T = 275$ K), which was derived from the Arrhenius expression (eq 18) obtained in this work. Globally, τ_{OH} was estimated to be more than 20 days. Sulbaek Andersen et al.[5] estimated an atmospheric lifetime for CF_3CF_2CHO of 40 days due to reaction with OH using their rate coefficient at 296 K and relative to CH_3CCl_3. The difference between our lifetime estimation and that of Sulbaek Andersen et al.[5] arises from the T-dependences of k_{OH} for CH_3CCl_3 and CF_3CF_2CHO. While k_{OH} for CF_3CF_2CHO decreases around 15% from 296 K to 275 K (see Table 3), k_{OH} for CH_3CCl_3 diminishes from 10^{-14} cm^3 molecule^{-1} s^{-1} (at 296 K) to 6.5×10^{-15} cm^3 molecule^{-1} s^{-1} (at 275 K). This difference in both k_{OH} makes that the lifetime for CF_3CF_2CHO estimated by Sulbaek Andersen et al.[5] be higher than that reported here at 275 K. For that reason, it is important to determine the temperature dependence of k_{OH}.

$\tau_{h\nu}$ for CF_3CF_2CHO was estimated in this work for a given altitude ($z = 3.5$ km) and zenith angle ($\theta = 16°$ corresponding to Ciudad Real (Spain) in summer midday) as the reciprocal of the photolysis rate coefficient, $J(z,\theta)$. An estimate of $J(z,\theta)$ can be obtained from eq 20:

$$J(z, \theta) \approx \sum \Phi_\lambda \sigma_\lambda F_{\lambda,solar}(z, \theta) \Delta\lambda \tag{20}$$

$F_{\lambda,solar}(z,\theta)$ is the spectral solar actinic flux at the simulated atmospheric conditions and was calculated by using the TUV radiative transfer model (4.1 version)[36] according to the procedure previously used.[14,19]

The importance of CF_3CF_2CHO photolysis in the atmosphere is still uncertain. The lack of wavelength and pressure dependence studies of Φ_λ makes difficult to accurately determine $J(z,\theta)$. In the absence of quantum yield measurements, Sulbaek Andersen et al.[5,37] reported that $\tau_{h\nu}$ for CF_3CF_2CHO was likely to be of a few weeks by similarity with that of $C_2F_5C(O)CF(CF_3)_2$.[7,14] This implies that removal of CF_3CF_2CHO by reaction with OH radicals is more important than by UV photolysis. In contrast, Chiappero et al.[7] estimated that $\tau_{h\nu}$ was less than 2 days at 40° latitude, assuming a constant photolysis quantum yield of 0.11 (i.e., independent of pressure and wavelength). Up to now, Chiappero et al.[7] reported $\Phi_{\lambda=254 \text{ nm}}$ for perfluoropropanal at 700 Torr of N_2/NO to be (0.81 ± 0.09). At this total pressure (of air, in our case), a $\Phi_{\lambda=308 \text{ nm}}$ of 0.32 was derived from eq 8. Therefore, Φ_λ for CF_3CF_2CHO seems to increase as the excitation energy increases, similarly to CF_3CH_2CHO.

In this work, the wavelength dependence of the absorption cross sections from Table S1 were used in the $J(z,\theta)$ calculation. At 700 Torr, we can assume an exponential decrease from 254 to 308 nm ($\Phi_{\lambda=308 \text{ nm}} = 0.32$, this work). It is expected that Φ_λ also decreases exponentially at other wavelengths. Assuming this, $J(z,\theta)$ for $z = 3.5$ km, where $T = 275$ K (an average temperature for the troposphere) was 7.90×10^{-5} s^{-1}, i.e., $\tau_{h\nu}$ is expected to be 3.5 h. A realistic evaluation of the OH chemistry and photolysis contribution to the atmospheric lifetime of CF_3CF_2CHO requires the use of 2D photochemical models. Even so, the tropospheric fate of the CF_3CF_2CHO depends on where it is formed and/or emitted. For instance, in the planetary boundary layer the OH chemistry

might be a very efficient sink for CF_3CF_2CHO. In contrast, an efficient photolytical removal of CF_3CF_2CHO is expected to occur at relatively high altitudes where the fluorinated aldehyde could be transported by direct-turbulent transfer.

5. CONCLUSIONS

The present kinetic and photochemical study reports information of atmospheric interest for CF_3CF_2CHO. The determination of the absorption cross sections in UV and IR regions (σ_λ and $\sigma(\tilde{\nu})$) is presented. Photolysis quantum yields at 308 nm ($\Phi_{\lambda=308 \text{ nm}}$) as a function of pressure (75−760 Torr) are reported. Moreover, the stable products formed from the radicals formed in the photolysis of CF_3CF_2CHO at this wavelength (CF_3CFO and F_2CO) have been quantified and their molar yields have been determined. Rate coefficients for the reaction with OH radicals (k_1) have been also presented as a function of temperature.

Degradation of CF_3CF_2CHO initiated by OH radicals is expected to occur in several weeks. Photolysis of CF_3CF_2CHO in the actinic region could be a major contribution to its atmospheric removal, even more important than OH radical reaction. Photochemical degradation of CF_3CF_2CHO mainly forms CF_3CFO and F_2CO, which can undergo heterogeneous reactions on aqueous surfaces. Thus, the environmental impact of degradation of the secondary pollutant CF_3CF_2CHO is not expected to be important. It will finally depend on the emissions of its precursors, $CF_3CF_2CH\!=\!CH_2$ and $CF_3CF_2CH_2OH$.

■ ASSOCIATED CONTENT

ⓈSupporting Information

Tables S1 and S2 show UV and IR absorption cross sections determined in this work. Figure S1 shows the Beer−Lambert Law plots at several wavelengths in the UV region. Figure S2 shows some temporal profiles of the LIF signal from OH radicals. This material is available free of charge via the Internet at http://pubs.acs.org.

■ AUTHOR INFORMATION

Corresponding Author
*Phone: 34 926 29 53 27; fax: 34 926 29 53 18; e-mail: Jose. Albaladejo@uclm.es.

Present Address
§Department of Chemistry, University of Toronto, 80 St. George, Toronto, ON, Canada M5S 3H6.

Notes
The authors declare no competing financial interest.

■ ACKNOWLEDGMENTS

■ REFERENCES

(1) Montzka, S. A.; Fraser, P. J. (lead authors). Scientific Assessment of Ozone Depletion: 2002. In *Global Ozone Research and Monitoring*

Project - Report No. 47; World Meteorological Organization: Geneva, Switzerland, 2003; Chapter 1.

(2) Daniel, J. S.; Velders, G. J. M. (lead authors). Scientific Assessment of Ozone Depletion: 2006. In *Global Ozone Research and Monitoring Project - Report No. 50*; World Meteorological Organization: Geneva, Switzerland, 2007; Chapter 8.

(3) Hurley, M. D.; Wallington, T. J.; Sulbaek Andersen, M. P.; Ellis, D. A.; Martin, J. W.; Mabury, S. A.. Atmospheric Chemistry of Fluorinated Alcohols: Reaction with Cl Atoms and OH Radicals and Atmospheric Lifetimes. *J. Phys. Chem. A* **2004**, *108*, 1973−1979.

(4) Vésine, E.; Bossoutrot, V.; Mellouki, A.; Le Bras, G.; Wenger, J.; Sidebottom, H. Kinetics and Mechanistic Study of OH- and Cl-Initiated Oxidation of Two Unsaturated HFCs: $C_4F_9CH=CH_2$ and $C_6F_{13}CH=CH_2$. *J. Phys. Chem. A* **2000**, *104*, 8512−8520.

(5) Sulbaek Andersen, M. P.; Hurley, M. D.; Wallington, T. J.; Ball, J. C.; Martin, J. W.; Ellis, D. A.; Mabury, S. A.; Nielsen, O. J. Atmospheric Chemistry of C_2F_5CHO: Reaction with Cl Atoms and OH Radicals, IR Spectrum of $C_2F_5C(O)O_2NO_2$. *Chem. Phys. Lett.* **2003**, *379*, 28−36.

(6) Lau, C.; Anitole, K.; Hodes, C.; Lai, D.; Pfahles, A.; Seed, J. Perfluoroalkyl Acids: A Review of Monitoring And Toxicological Findings. *Toxicol. Sci.* **2007**, *99*, 366−394.

(7) Chiappero, M. S.; Malanca, F. E.; Argüello, G. A.; Wooldridge, S. T.; Hurley, M. D.; Ball, J. C.; Wallington, T. J.; Waterland, R. L.; Buck, R. C. Atmospheric Chemistry of Perfluoroaldehydes ($C_xF_{2x+1}CHO$) and Fluorotelomer Aldehydes ($C_xF_{2x+1}CH_2CHO$): Quantification of the Important Role of Photolysis. *J. Phys. Chem. A* **2006**, *110*, 11944−11953.

(8) Hashikawa, Y.; Kawasaki, M.; Waterland, R. L.; Hurley, M. D.; Ball, J. C.; Wallington, T. J.; Sulbaek Andersen, M. P.; Nielsen, O. J. Gas Phase UV and IR Absorption Spectra of $C_xF_{2x+1}CHO$ (x = 1−4). *J. Fluorine Chem.* **2004**, *125*, 1925−1932.

(9) Solignac, G.; Mellouki, A.; Le Bras, G.; Barnes, I.; Benter, T. Reaction of Cl Atoms with $C_6F_{13}CH_2OH$, $C_6F_{13}CHO$, and C_3F_7CHO. *J. Phys. Chem. A* **2006**, *110*, 4450−4457.

(10) Solignac, G.; Mellouki, A.; Le Bras, G.; Yujing, M.; Sidebottom, H. The Gas Phase Tropospheric Removal of Fluoroaldehydes ($C_xF_{2x+1}CHO$, x = 3, 4, 6). *Phys. Chem. Chem. Phys.* **2007**, *9*, 4200−4210.

(11) Sellevåg, S. R.; Kelly, T.; Sidebottom, H.; Nielsen, C. J. A Study of the IR And UV-Vis Absorption Cross-Sections, Photolysis and OH-Initiated Oxidation of CF_3CHO and CF_3CH_2CHO. *Phys. Chem. Chem. Phys.* **2004**, *6*, 1243−1252.

(12) Chiappero, M. S.; Argüello, G. A.; Hurley, M. D.; Wallington, T. J. Atmospheric Chemistry of n-$C_6F_{13}CH_2CHO$: Formation from n-$C_6F_{13}CH_2CH_2OH$, Kinetics and Mechanisms of Reactions with Chlorine Atoms and OH Radicals. *J. Phys. Chem. A* **2010**, *114*, 6131−6137.

(13) Antiñolo, M.; Jiménez, E.; Notario, A.; Martínez, E.; Albaladejo, J. Tropospheric Photooxidation of CF_3CH_2CHO and $CF_3(CH_2)_2CHO$ Initiated by Cl Atoms and OH Radicals. *Atmos. Chem. Phys.* **2010**, *10*, 1911−1922.

(14) Antiñolo, M.; Jiménez, E.; Albaladejo, J. UV Absorption Cross Sections Between 230 and 350 nm and Pressure Dependence of the Photolysis Quantum Yield at 308 nm of CF_3CH_2CHO. *Phys. Chem. Chem. Phys.* **2011**, *13*, 15936−15946.

(15) Antiñolo, M.; Jiménez, E.; Albaladejo, J. Photochemistry of $CF_3(CH_2)_2CHO$ in Air: UV Absorption Cross Sections Between 230 and 340 nm and Photolysis Quantum Yields at 308 nm. *J. Photochem. Photobiol., A* **2012**, *231*, 33−40.

(16) Husted, D. R.; Ahlbrecht, A. H. The Chemistry of the Perfluoro Acids and Their Derivatives. III. The Perfluoro Aldehydes. *J. Am. Chem. Soc.* **1952**, *74*, 5422−5425.

(17) Braid, M.; Iserson, H.; Lawlor, F. E. An Improved Synthesis of Perfluoroaldehydes. *J. Am. Chem. Soc.* **1954**, *76*, 4027−4027.

(18) Jiménez, E.; Lanza, B.; Garzón, A.; Ballesteros, B.; Albaladejo, J. Atmospheric Degradation of 2-Butanol, 2-Methyl-2-butanol, and 2,3-Dimethyl-2-butanol: OH Kinetics and UV Absorption Cross Sections. *J. Phys. Chem. A* **2005**, *109*, 10903−10909.

(19) Lanza, B.; Jiménez, E.; Ballesteros, B.; Albaladejo, J. Absorption Cross Section Determination of Biogenic C_5-Aldehydes in the Actinic Region. *Chem. Phys. Lett.* **2008**, *454*, 184−189.

(20) Jiménez, E.; Antiñolo, A.; Ballesteros, B.; Martínez, E.; Albaladejo, J. Atmospheric Lifetimes and Global Warming Potentials of $CF_3CH_2CH_2OH$ and $CF_3(CH_2)_2CH_2OH$. *Chem. Phys. Chem.* **2010**, *11*, 4079−4087.

(21) Antiñolo, M.; González, S.; Ballesteros, B.; Albaladejo, J.; Jiménez, E. Laboratory Studies of $CHF_2CF_2CH_2OH$ and $CF_3CF_2CH_2OH$: UV and IR Absorption Cross Sections and OH Rate Coefficients between 263 and 358 K. *J. Phys. Chem. A* **2012**, *116*, 6041−6050.

(22) Moortgat, K.; Meyrahn, H.; Warneck, P. Photolysis of Acetaldehyde in Air: CH_4, CO and CO_2 Quantum Yields. *Chem. Phys. Chem.* **2010**, *11*, 3896−3908.

(23) Atkinson, R.; Baulch, D. L.; Cox, R. A.; Crowley, J. N.; Hampson, R. F.; Hynes, R. G.; Jenkin, M. E.; Rossi, M. J.; Troe, J. Evaluated Kinetic and Photochemical Data for Atmospheric Chemistry: Volume II − Gas Phase Reactions of Organic Species. *Atmos. Chem. Phys.* **2006**, *6*, 3625−4055.

(24) Albaladejo, J.; Ballesteros, B.; Jiménez, E.; Martín, P.; Martínez, E. A PLP-LIF Kinetic Study of the Atmospheric Reactivity of a Series of C_4-C_7 Saturated and Unsaturated Aliphatic Aldehydes with OH. *Atmos. Environ.* **2002**, *36*, 3231−3239.

(25) Jiménez, E.; Ballesteros, B.; Martínez, E.; Albaladejo, J. Tropospheric Reaction of OH with Selected Linear Ketones: Kinetic Studies Between 228 and 405 K. *Environ. Sci. Technol.* **2005**, *39*, 814−820.

(26) Jiménez, E.; Lanza, B.; Antiñolo, M.; Albaladejo, J. Photo-oxidation of Leaf-Wound Oxygenated Compounds, 1-Penten-3-ol, (Z)-3-Hexen-1-ol, and 1-Penten-3-one, Initiated by OH Radicals and Sunlight. *Environ. Sci. Technol.* **2009**, *43*, 1831−1837.

(27) Atkinson, R.; Baulch, D. L.; Cox, R. A.; Crowley, J. N.; Hampson, R. F.; Hynes, R. G.; Jenkin, M. E.; Rossi, M. J.; Troe, J. Evaluated Kinetic And Photochemical Data For Atmospheric Chemistry: Volume I − Gas Phase Reactions of O_x, HO_x, NO_x and SO_x Species. *Atmos. Chem. Phys.* **2004**, *4*, 1461−1738.

(28) Borkowski, R. P.; Ausloos, P. The Vapor Phase Fluorescence and Its Relationship to the Photolysis of Propionaldehyde and the Butyraldehydes. *J. Am. Chem. Soc.* **1962**, *84*, 4044−4048.

(29) Pritchard, G. O.; Miller, G. H.; Foote, J. K. The Hydrogen-Abstraction Reactions in the Photolysis of Pentafluoropropanal and Heptafluorobutanal. *Can. J. Chem.* **1962**, *40*, 1830−1835.

(30) Barnes, I. Personal communication.

(31) Hurley, M. D.; Wallington, T. J.; Javadi, M. S.; Nielsen, O. J. Atmospheric Chemistry of $CF_3CF=CH_2$: Products and Mechanisms of Cl Atom and OH Radical Initiated Oxidation. *Chem. Phys. Lett.* **2008**, *450*, 263−267.

(32) Hurley, M. D.; Ball, J. C.; Wallington, T. J.; Sulbaek Andersen, M. P.; Nielsen, O. J.; Ellis, D. A.; Martin, J. W.; Mabury, S. A. Atmospheric Chemistry of n-$C_xF_{2x+1}CHO$ (x = 1, 2, 3, 4): Fate of n-$C_xF_{2x+1}C(O)$ Radicals. *J. Phys. Chem. A* **2006**, *110*, 12443−12447.

(33) Setokuchi, O.; Kutsuna, S.; Sato, M. A Theoretical Study of Thermal Decomposition of CF_3CO, C_2F_5CO and C_3F_7CO. *Chem. Phys. Lett.* **2006**, *429*, 360−364.

(34) Atkinson, R.; Arey, J. Atmospheric Degradation of Volatile Organic Compounds. *Chem. Rev.* **2003**, *103*, 4605−4638.

(35) Krol, M.; van Leeuwen, P. J.; Lelieveld, J. Global OH Trend Inferred from Methylchloroform Measurements. *J. Geophys. Res. Atmos.* **1998**, *103*, 10697−10711.

(36) Madronich, S., Flocke, S. The role of solar radiation in atmospheric chemistry. In *Handbook of Environmental Chemistry*; Boule, P., Ed.; Springer-Verlag: Heidelberg, 1999; pp 1−26.

(37) Atkinson, R.; Baulch, D. L.; Cox, R. A.; Crowley, J. N.; Hampson, R. F.; Hynes, R. G.; Jenkin, M. E.; Rossi, M. J.; Troe, J. Evaluated Kinetic and Photochemical Data for Atmospheric Chemistry: Volume III − Gas Phase Reactions of Inorganic Halogens. *Atmos. Chem. Phys.* **2008**, *8*, 4141−4496.